

# CP violation in semi-leptonic decays of the top quark within MSSM

Xiao-Jun Bi and Yuan-Ben Dai

*Institute of Theoretical Physics, Academia Sinica,  
P.O.Box 2735, Beijing 100080, P. R. China*

## Abstract

We calculate the CP-violating effects in the top quark semi-leptonic three body decays induced by the supersymmetric CP-odd phase of the top squark trilinear soft breaking term  $\arg(A_t)$ . The light top squark mass is assumed to be close to the top quark mass  $m_{\tilde{t}} \sim m_t$ . The CP-conserving phase is provided by the  $\chi^+$  and  $\chi^0$  cut. We find that the partial rate asymmetry is in the 0.1% level. In the most favorable parameter region the decay rate asymmetry can reach up to 0.55%.

## 1 Introduction

Top quark physics is sensitive to new physics, which may exist near the electro-weak scale, due to its large mass. Experimental and theoretical research about CP violation in top sector is one way to reveal new physics. To study the top quark CP-odd effects has its own advantage that the uncertainties coming from hardron matrix elements can be avoided.

If  $m_t$  is near to  $m_{newphysics}$ , the CP-asymmetry effects in top quark decays can be induced by new particles. Until now a lot of works about CP-asymmetry effects in the top quark decays[1] have been done within the supersymmetric model. Most of those works have made the assumption that the mass of the light top squark is much smaller than that of the top quark. B.Grzadkowski and W.Y.Keung calculated the CP violating effects induced by  $\tilde{t}\tilde{b}\tilde{g}$ -loop[2]. This contribution requires the condition  $m_{\tilde{t}} + m_{\tilde{g}} < m_t$ , which has already been excluded. E.Christova and M.Fabbrichesì computed the effects induced by  $\tilde{t}\tilde{b}\chi^0$ -loop[3] which requires  $m_{\tilde{t}} + m_{\chi^0} < m_t$ . S. Bar-Shalom *et al* gave the CP asymmetry in top quark decay induced by  $\tilde{t}\chi^+\chi^0$ . It is at best 0.3% when light stop mass is between  $\sim 50GeV$  and  $\sim 70GeV$ [4].

However, if the light top squark mass  $m_{\tilde{t}_1}$  is approximately as heavy as the top quark, CP–asymmetry effect in top quark two body decay induced by supersymmetric CP–odd phase will not be observable because the top squark can not run on shell to produce the necessary absorptive cut. In this work we considered this case under the assumption that the light chargino is much lighter than  $m_{\tilde{t}_1}$ . Under this condition, the  $\chi^0$  ( which is always assumed to be the LSP ) and  $\chi^+$  can provide necessary absorptive cut in top quark three body decays, such as in the process  $t \rightarrow b\nu_\tau\tau$  considered in the work. These two particles can be on shell in the top quark three body decay loop diagrams when the invariant mass of the lepton pair is sufficiently large. To our knowledge, a study on CP asymmetry in the top quark three body decays is missed in literature.

In the present work the mass of the light top squark is assumed to be above 140GeV. Taking into account the direct experimental limit on super particles[5] and the indirect limit coming from neutron EDM limit[6], we take  $\mu$  to be real and , the lightest neutralino to be above 30GeV and the lighter chargino to be above 65GeV. The large mass of stop leads to relatively small CP violating effects. Nevertheless, the CP–odd effects can reach up to 0.55% in the most favorable parameter space.

The paper is organized as following: in Sec. 2 we analyze the possible new CP violating sources in MSSM and present our simplifying assumptions in calculation. In sec. 3 we sketch the main steps of our calculations. In sec. 4 we present our numerical results and in sec. 5 and sec. 6 we discuss and summarize our results. The mass matrices for charginos, neutralinos and squarks are given in appendix A. In appendix B we give the relevant pieces of the Lagrangian for our calculations and some analytic results are presented in appendix C.

## 2 CP violating phases in the low energy supersymmetric model

The most general form of the low energy Lagrangian of MSSM[7, 8], which is  $SU(3) \times SU(2) \times U(1)$  gauge invariant and does not violate the SM conservation laws, can be written as

$$\mathcal{L} = \text{kinetic terms} + \int d^2\theta W + \mathcal{L}_{\text{soft}} \quad . \quad (1)$$

The superpotential  $W$  is given by

$$W = \epsilon_{ij}(\mu\hat{H}_i^1\hat{H}_j^2 + l^{IJ}\hat{H}_i^1\hat{L}_j^I\hat{R}^J + u^{IJ}\hat{H}_i^2\hat{Q}_j^I\hat{U}^J + d^{IJ}\hat{H}_i^1\hat{Q}_j^I\hat{D}^J) \quad (2)$$

where  $\epsilon_{12} = -1$ . The hat ‘ $\hat{\phantom{x}}$ ’ indicates that the corresponding letter represents a superfield. The capital indices I,J denote generations. i,j refer to the components of a SU(2) doublet. The l,d,u are the Yukawa coupling matrices. The soft breaking terms can be divided into three pieces,

$$\mathcal{L}_{\text{soft}} = \mathcal{L}_{\text{scalar}} + \mathcal{L}_{\text{gaugino}} + \mathcal{L}_{\text{trilinear}} \quad . \quad (3)$$

These are the scalar particle mass terms, gaugino mass terms and the trilinear soft breaking terms respectively. They are given by

$$\begin{aligned} \mathcal{L}_{\text{scalar}} = & \epsilon_{ij}\mu_s H_i^1 H_j^2 - m_{H_1}^2 |H_i^1|^2 - m_{H_2}^2 |H_i^2|^2 - (m_L^2)^{IJ} L_i^{I*} \cdot L_i^J - \\ & (m_R^2)^{IJ} R^{I*} \cdot R^J - (m_Q^2)^{IJ} Q_i^{I*} \cdot Q_i^J - \\ & (m_D^2)^{IJ} D^{I*} \cdot D^J - (m_U^2)^{IJ} U^{I*} \cdot U^J \quad , \end{aligned} \quad (4)$$

$$\mathcal{L}_{\text{gaugino}} = \frac{1}{2}(m_1 \lambda_B \lambda_B + m_2 \lambda_W^i \lambda_W^i + m_3 \lambda_G^a \lambda_G^a) + H.C. \quad , \quad (5)$$

$$\begin{aligned} \mathcal{L}_{\text{trilinear}} = & \epsilon_{ij} ( (A_E l)^{IJ} H_i^1 L_j^I R^J + (A_D d)^{IJ} H_i^1 Q_j^I D^J + \\ & (A_U u)^{IJ} H_i^2 Q_j^I U^I ) + H.C. \quad , \end{aligned} \quad (6)$$

where  $m_1, m_2, m_3$  are U(1), SU(2) and SU(3) gauginos masses respectively. Fields in  $\mathcal{L}_{\text{scalar}}$  and  $\mathcal{L}_{\text{trilinear}}$  are scalar components of the corresponding superfields.

In general, all the coupling parameters in the above expressions except those of the diagonal terms in  $\mathcal{L}_{\text{scalar}}$  may be complex which may be the CP violating sources. However, not all of them are physical and, even the physical parameters are too many to be disposed of. In actual calculations, simplifying assumptions must be made. We get the physical CP violating phases by the following steps.

First, we take the GUT assumption that the  $m_i$ s are universal at the GUT scale and can be set real by a phase rotation[9]. Thus, the  $m_i$ s are real at any scale. Second, we adjust the global phase between the two Higgs superfields so that  $\mu_s$  is real. This adjustment makes the two vacuum expectation values of the neutral Higgs fields  $v_1, v_2$  real[8]. After the adjustment the phases of the two Higgs superfields are fixed and  $\mu$  is complex in general. Third,  $l^{IJ}$ ,  $d^{IJ}$ , and  $u^{IJ}$  in the superpotential are diagonalized and the unphysical phases are absorbed by quark superfields similar to that done in the standard model. This leaves a CP violating phases  $\delta_{KM}$  in the Kinetic terms after the superfield are redefined. Fourth, to suppress the FCNC process in the SUSY extension of SM, as an approximation we require that all the matrices in  $\mathcal{L}_{\text{soft}}$ ,  $m_L^2$ ,  $m_R^2$ ,  $m_Q^2$ ,  $m_U^2$ ,  $m_D^2$ ,  $A_U$ ,  $A_D$  and  $A_E$  are flavor diagonal in the basis where  $l^{IJ}$ ,  $d^{IJ}$  and  $u^{IJ}$  are diagonal (flavor alignment[10]). Then the Hermitian matrices in  $\mathcal{L}_{\text{scalar}}$  are now all real. The phases of all squarks are fixed after the third step. Therefore,  $A_D$ ,  $A_U$  are generally complex. In conclusion,  $\delta_{KM}$ ,  $\arg(\mu)$ ,  $\arg(A_D)$ s and  $\arg(A_U)$ s are the CP violating phases in the low energy supersymmetric model under our assumptions.

$\arg(\mu)$  can not be larger than the order  $\sim \mathcal{O}(10^{-2} - 10^{-3})$  by the constraint from the experimental limit of the neutron EDM[6]. In our calculation, we always take  $\mu$  to be real and thus

no CP-violating effects are induced by  $\mu$ . The CP violating effects induced by  $A_{D,U}$  are greatly suppressed because they are proportional to the masses of the corresponding quarks which can be neglected compared with the squark mass parameters in  $\mathcal{L}_{\text{scalar}}$  except that induced by  $A_t$  which is associated with the top quark(see the form of squark mass matrices in (A.8) and (A.9) in Appendix A). Thus,  $\arg(A_t)$  is the only new CP violating source in our calculation.

After the interaction terms in the potential are diagonalized, the MSSM Lagrangian will be expressed by mass eigenstates instead of gauge eigenstates. The CP violating phases are then transferred to the gauge interaction vertices (see Appendix B for related Lagrangian pieces). This is reflected by mixing matrices in the interaction vertices. The mixing matrices  $Z^+, Z^-, Z_N$  which diagonalize charginos and neutralinos are real if  $\mu$  is taken real. The mixing matrices  $Z_t$  for the top squark is in general complex due to the complexity of  $A_t$ . This implies that the CP violating effects comes from  $\arg(A_t)$ . The mixing matrices will be discussed in detail in the appendix A.

### 3 Calculation

We now discuss the CP violating effects in the process  $t \rightarrow b\nu_\tau\bar{\tau}$ , which corresponds to diagrams in Fig.1, within the MSSM framework. First denote the invariant mass of  $\bar{\tau}$  and  $\nu_\tau$  as  $\sqrt{q^2}$ , where  $q = p_{\nu_\tau} + p_{\bar{\tau}}$ .  $p_{\nu_\tau}$  and  $p_{\bar{\tau}}$  are the four-momenta of  $\nu_\tau$  and  $\bar{\tau}$ . We calculated the CP asymmetry when  $q^2 > m_W^2$ . This condition opens a new window so that  $\chi^+$  and  $\chi^0$  cut may give an absorptive part to the amplitudes for loop diagrams as depicted in Fig.2.

Several points should be indicated at the moment.

- (1). There should be a minus sign in front of the amplitudes for box diagrams relative to that for triangle diagrams. <sup>1</sup>
- (2). There are two kinds of box diagrams. One of them, Fig.2a and 2b, is fermion number nonconservative[7].
- (3). We have assumed that the absorptive part of the amplitude for the loop diagrams are induced by  $\chi^0 \chi$  cut[12].  $\tilde{t}$  or  $\tilde{\tau}$  can also be on shell and give new contribution to absorptive part under the condition  $m_{\tilde{t}} + m_{\chi^0} < m_t$  or  $m_\chi > m_{\tilde{\tau}}$ , respectively. We excluded these two cases for simplicity for the following reasons. Under our assumption about the stop mass,  $m_{\tilde{t}} + m_{\chi^0} < m_t$  can be satisfied only in very narrow SUSY parameter region which is simply excluded in our calculation.  $m_\chi > m_{\tilde{\tau}}$  means the CP-odd effect will appear as  $\sqrt{q^2} > 160\text{GeV}$  (we take  $m_{\tilde{\nu}} = 130\text{GeV}$ ) which has too small branch ratio and can be ignored.

---

<sup>1</sup> This can be explained by that we can get the amplitude for Fig.2e from that for Fig.2a by interchanging the field operators of  $\chi^-$  and  $\bar{\tau}$  at two ends of the  $\tilde{\tau}$  propagator and simultaneously changing  $\tilde{\tau}$  to W boson in the Wick contraction procedure. The interchange of two fermion operators gives the minus sign. An analogous case on QED can be found in [11].

Two quantities are defined to represent the CP–asymmetry effects,

$$\begin{aligned}
A_{CP}^{t,e} &= \frac{\Gamma - \bar{\Gamma}}{\Gamma + \bar{\Gamma}} \\
&= \frac{\int_{L_{t,e}}^{m_t^2} dq^2 \frac{d\Gamma(q^2)}{dq^2} - \int_{L_{t,e}}^{m_t^2} dq^2 \frac{d\bar{\Gamma}(q^2)}{dq^2}}{\int_{L_{t,e}}^{m_t^2} dq^2 \frac{d\Gamma(q^2)}{dq^2} + \int_{L_{t,e}}^{m_t^2} dq^2 \frac{d\bar{\Gamma}(q^2)}{dq^2}} ,
\end{aligned} \tag{7}$$

$$L_t = (m_\chi + m_{\chi^0})^2, \tag{8}$$

$$L_e = (100\text{GeV})^2, \tag{9}$$

where  $\frac{d\Gamma(q^2)}{dq^2}$  and  $\frac{d\bar{\Gamma}(q^2)}{dq^2}$  are differential widths of top quark and top anti–quark.  $A_{CP}^t$  reflects the theoretical CP–odd effect appearing when the invariant mass  $\sqrt{q^2}$  is above the threshold.  $A_{CP}^e$  reflects the experimental CP–asymmetry effect when we measure the decay events with  $q^2 > L_e$ , which is fixed to be  $(100\text{GeV})^2$  in the work.

We have only considered the contribution to the denominator in Eq. 7 from the tree–level diagrams which gives  $\Gamma = \bar{\Gamma}$ . The nominator comes from the interference of the one–loop diagrams with the tree–level diagram, as

$$\begin{aligned}
\Delta\Gamma &= \Gamma - \bar{\Gamma} = \Delta|M|^2 \cdot \text{phase space} \\
&= (|M|^2 - |\bar{M}|^2) \cdot \text{phase space} .
\end{aligned} \tag{10}$$

The three body final state “phase space” is

$$\begin{aligned}
\text{phase space} &= \frac{1}{2m_t} \int \frac{d^3p_b}{(2\pi)^3 2E_b} \frac{d^3p_{\bar{\tau}}}{(2\pi)^3 2E_{\bar{\tau}}} \frac{d^3p_{\nu_\tau}}{(2\pi)^3 2E_{\nu_\tau}} \\
&\quad \cdot (2\pi)^4 \delta(p_t - p_b - p_{\bar{\tau}} - p_{\nu_\tau}).
\end{aligned} \tag{11}$$

The above expression multiplied by a  $\delta((p_{\bar{\tau}} + p_{\nu_\tau})^2 - q^2)$  gives the phase space for fixed  $q^2$ .  $M$ ,  $\bar{M}$  are the amplitudes for the process  $t \rightarrow b\nu_\tau\bar{\tau}$  and its CP conjugate process  $\bar{t} \rightarrow \bar{b}\bar{\nu}_\tau\tau$ , respectively.

$M$  can be expressed as

$$M = aA_1 + \sum_i b^i A_2^i, \tag{12}$$

where the two terms come from tree–level and one–loop diagrams respectively.  $a$ ,  $b^i$  contain the CP–violating phases both from KM matrix element  $V_{tb}$  and from stop mixing matrix elements  $Z_t^{ij}$ .  $A_2^i$  develops an absorptive part for  $q^2$  beyond the threshold.  $\bar{M}$  can be expressed as

$$\bar{M} = a^*A_1 + \sum_i b^{i*} A_2^i. \tag{13}$$

So, we have

$$\Delta|M|^2 = -4 \sum_i \text{Im}(a^*b^i) \text{Im}(A_2^i A_1^*). \tag{14}$$

$ImA_2^i$  is given by Cutkosky rule,

$$\sum_i b^i ImA_2^i = \frac{1}{2} \int d\Phi \hat{A}(t \rightarrow b\chi^+\chi^0) \hat{A}(\chi^+\chi^0 \rightarrow \bar{\tau}\nu_\tau), \quad (15)$$

where

$$d\Phi = \int \frac{d^3k}{(2\pi)^3 2E_{\chi^0}} \frac{d^3k'}{(2\pi)^3 2E_{\chi^+}} \cdot (2\pi)^4 \delta(p_t - p_b - k - k'), \quad (16)$$

are the phase space of  $\chi^0, \chi^+$  as they are on shell.  $k, k'$  are the four-momenta of  $\chi^0$  and  $\chi^+$ , respectively. After summing up all spins of external particles we get, e.g., the interference term of Fig.2a and the tree-level graph of the form

$$\begin{aligned} \frac{1}{2} \sum_{\text{spin}} \Delta|M|^2(a) &= -2 \sum_i Im(a^*b^i) \sum_{\text{spin}} Im(A_2^i A_1^*) \\ &= \frac{g^6}{q^2 - m_W^2} \frac{1}{(2\pi)^2} \int \frac{d^3k}{E} \delta((q-k)^2 - m_\chi^2) \frac{\sum_i \mathcal{X}_a^i F_i}{\mathcal{P}_1 \mathcal{P}_2} \end{aligned} \quad (17)$$

where we have introduced  $\mathcal{X}_a^i$ s to represent quantities like  $Im(a^*b^i)$  in Eq. 14 arising from the SUSY couplings and the corresponding  $F_i$ s to represent quantities like  $Im(A_2 A_1^*)$  which are Lorentz invariant functions of the four-momenta of  $\chi^0, b, \bar{\tau}$  and  $\nu_\tau$ .  $\mathcal{P}_1$  and  $\mathcal{P}_2$  are denominators of the two boson propagators in the loop graphs. Note that the SM phase from  $V_{tb}$  is cancelled in the interference of the tree diagram and the one-loop diagrams.

We get the analytic expressions for  $\frac{1}{2} \sum_{\text{spin}} \Delta|M|^2$  by integrating the phase space of  $\chi^0$  and  $\chi^+$  in  $\vec{q} = 0$  system. The analytic results are given in appendix C. By expressing the formulae in Lorentz invariant form, we translate the formulae to the top quark rest system. In this system the final state three body phase space integration is implemented numerically.

All the  $\mathcal{X}^i$ s for each graphs are proportional to  $\xi_t^j$  (for detail expressions of  $\mathcal{X}^i$ s, see Appendix C), so, we can write

$$A_{CP} = \xi_t^1 \cdot f_{CP}, \quad (18)$$

where

$$\xi_t^j = Im Z_t^{1j*} Z_t^{2j} = \frac{(-1)^j}{2} \sin(2\theta_t) \sin \phi_t, \quad (19)$$

$\theta_t$  and  $\phi_t$  are given in (A.13) and (A.9) of Appendix A. In terms of parameters in the top squark mass matrix we get that

$$\xi_t^j = \frac{(-1)^{j-1} m_t \cdot Im A_t}{\sqrt{\Delta}} \quad (20)$$

From the expression of  $\Delta$  in (A.13) of Appendix A we can see that  $|\xi_t^i|$  can be as large as  $\frac{1}{2}$  when the following conditions are satisfied at the same time, i.e.,  $L_f = R_f, \mu = 0$  and  $A_t$  is purely imaginary. This is certainly difficult to reach.

## 4 Numerical results

We now turn to our main numerical results. The calculation is based on the low energy MSSM scenario whose parameter freedom has been greatly reduced as described in section 2. Another simplifying assumption taken in our calculation is the universal relationship between the gaugino masses, i.e.,  $m_1 = \frac{5}{3}m_2 \tan^2 \theta_W$ , where  $\theta_W$  is the weak mixing angle[13]. We write the parameters  $m_{\tilde{t}L}^2, m_{\tilde{t}R}^2$  in the top squark mass matrix as

$$m_{\tilde{t}L}^2 = M^2 - cm_t^2, \quad m_{\tilde{t}R}^2 = M^2 - 2cm_t^2 \quad (21)$$

where  $M$  is an arbitrary mass scale for scalar particles.

Neglecting the masses of  $\tau$  and quarks except top quark we are left with ten SUSY parameters, i.e.,  $\mu, m_2, \tan \beta, c, M, |A_t|, \arg(A_t), m_{\tilde{\tau}L}, m_{\tilde{\tau}R}$  and  $m_{\tilde{\nu}}$ . We take  $m_{\tilde{\tau}L} = m_{\tilde{\tau}R} = m_{\tilde{\nu}} = 130\text{GeV}$  to which the results are insensitive, and always take  $|A_t| = M, c = 0.1 \sim 1$ . The other free SUSY parameters are restricted by the experimental limits on the masses of super particles [5] and our assumption  $m_{\tilde{t}_1} \geq 140\text{GeV}$ . In particular, we take that,  $m_{\chi^0_1}$ , the mass of the lightest neutralino, is above  $30\text{GeV}$  and  $m_{\chi^{\pm}_1}$ , the mass of the light chargino, is above  $65\text{GeV}$ . Another limit for the parameter space is adopted for simplicity that we require  $m_{\chi^0_1} + m_{\chi^{\pm}_1} > 100\text{GeV}$  and  $m_{\chi^0_1} + m_{\tilde{t}_1} > m_t$ . The SM parameters are taken as  $m_t = 175\text{GeV}, |V_{tb}|^2 = 1, \alpha = \frac{1}{128}, m_W = 80.33\text{GeV}, \sin \theta_W = 0.232$  and  $m_b = m_\tau = 0$ .

A consequence of the above scenario, especially that  $\arg(\mu)=0$  and  $m_b = 0$  is that Figs.2c, 2d and 2f do not acquire any CP-violating phase. So only Figs.2a, 2b and 2e are considered. It is found numerically that more than 90% of contributions to  $A_{CP}$  come from the triangle diagram Fig.2e. Because of this, the results are not sensitive to the values of  $m_{\tilde{\tau}}$  and  $m_{\tilde{\nu}}$ .

We have studied the CP asymmetry,  $A_{CP}$ , as a function of SUSY parameters  $\arg(A_t), \mu, \tan \beta, m_2$  and  $m_{\tilde{t}_1}$ . In all the figures there are two curves for the same values of the fixed parameters of which the curve giving larger  $A_{CP}$  represents  $A_{CP}^t$  while that giving a smaller value represents  $A_{CP}^e$ .

In Fig.3 we show the  $A_{CP}$  as a function of  $\arg(A_t)$ . We can see that  $A_{CP}$  is approximately a sine function of  $\arg(A_t)$  as can be seen in Eq. 18 and Eq. 19.  $f_{CP}$  defined in Eq. 18 is plotted in Fig.4. We see that  $f_{CP}$  is just like a parabola. As a result  $A_{CP}$  does not reach its maximum when  $A_t$  is purely imaginary, rather, it is maximal at  $\arg(A_t) \approx \pm 0.7\pi$ .  $f_{CP}$  depends on  $\arg(A_t)$  through the top squark mass (see Appendix A).

In Figs.5–7, we plotted  $A_{CP}$  as a function of the Higgs mass parameter  $\mu$  for  $\tan \beta = 1.2, 5, 15$  respectively, for different values of  $m_2$ . The global feature of the three figures is that  $A_{CP}$  decrease dramatically as  $|\mu|$  increase. Notice that, in the high  $\tan \beta$  scenario  $A_{CP}$  becomes quite insensitive to the sign of  $\mu$ .  $A_{CP}$  is almost symmetric about  $|\mu|$  for  $\tan \beta = 15$ . However, as  $\tan \beta = 1.2$   $A_{CP}$  is not small only for minus  $\mu$ . Another feature of the figures is that for fixed  $\tan \beta$  and  $\mu$ ,  $A_{CP}^e$

decrease whereas  $A_{CP}^t$  increase as  $m_2$  become larger. The reason is evidently that the threshold varies with  $m_2$ .

The dependence of  $A_{CP}$  on  $\tan\beta$  is plotted in Fig.8 and Fig.9, for several values of  $m_2$  and for  $\mu = -70GeV$  and  $\mu = -50GeV$ , respectively. An interesting feature of these two figures is that  $A_{CP}^t$  decreases as  $\tan\beta$  increases whereas  $A_{CP}^e$  increases. This is because low  $\tan\beta$  gives strong Yukawa coupling for top quark so that we get large  $A_{CP}^t$ . However, large  $\tan\beta$  makes the threshold lower and thus elevates  $A_{CP}^e$ . So,  $A_{CP}^e$  prefers bigger  $\tan\beta$  in contrast to the situation in the top quark two body decays. As  $\tan\beta > 4$ , we can see from Fig.8 that  $A_{CP}^t$  is almost insensitive to  $\tan\beta$ .

The dependence of  $A_{CP}$  on  $m_2$  is plotted in Fig.10, for several values of  $\tan\beta$ . We can see that the major part of the curve  $A_{CP}^e$  falls into the region between 0.1%–0.2%. For  $\tan\beta = 2$ ,  $A_{CP}$  rises as  $m_2$  increases whereas for large  $\tan\beta$   $A_{CP}$  slightly drops as  $m_2$  increases.

Finally, we give the dependence of  $A_{CP}$  on the top squark mass in Fig.11 for  $\mu = -50GeV$ . It is found that  $A_{CP}$  depends essentially only on  $m_{\tilde{t}_1}$ , not separately on  $M$  and  $c$ .  $A_{CP}$  decreases with  $m_{\tilde{t}_1}$ , just as what has been expected. When  $m_{\tilde{t}_1}$  is around 140 GeV  $A_{CP}$  can reach up to 0.5%.

In summary,  $A_{CP}^e$  is around 0.1% level in the major part of the parameter space that we have discussed. In a very narrow region of the parameter space,  $A_{CP}^e$  can reach 0.5% level.

## 5 Discussion

We would like to point out two points in this section.

(1). The branch ratio for top quark decay drops rapidly when W boson is off shell. For  $\sqrt{q^2} > 100GeV$  the branch ratio for  $b\nu_\tau\tau$  final state is only about  $\frac{1}{1000}$  according to our calculation. However, as we have mentioned that the contributions to  $A_{CP}$  comes mainly from the triangle diagrams in Fig.2,  $A_{CP}$  for different final states have the same sign and approximately the same size. So we can make a combining analysis for the data of the three body CP asymmetries for different three fermion final states  $(\tau, \nu_\tau)$ ,  $(\mu, \nu_\mu)$ ,  $(e, \nu_e)$ , and all allowed three quark decays. The total branch ratio for top quark three body decay for  $\sqrt{q^2} > 100GeV$  can reach up to about  $\frac{1}{100}$ . However, there are CP asymmetries of the order  $(\frac{\alpha_s}{\pi})^2$  for three quark decays coming from gluon and gluino corrections, which may be of the same order as considered here. This needs to be studied further if one attempts to quantitatively compare the theory and experimental CP asymmetries for three quark decays.

(2). The total width of top and anti-top quark are equal  $\Gamma = \bar{\Gamma}$  due to CPT theorem. The



following relation holds

$$\Gamma(t \rightarrow bf\bar{f}') - \bar{\Gamma}(\bar{t} \rightarrow \bar{b}\bar{f}f') = - \left( \Gamma(t \rightarrow b\chi^0\chi^+) - \bar{\Gamma}(\bar{t} \rightarrow \bar{b}\chi^0\chi^-) \right)_{f\bar{f}'}, \quad (22)$$

where  $f\bar{f}'$  represent all the  $W$  boson decay products mentioned above and the RHS of Eq. 22 denotes the CP asymmetry from the diagrams with  $f\bar{f}'$  as intermediate states. The relation can be easily seen from the Feynman diagrams representing these two processes in Fig.1, 2 and Fig.12.

The four interference terms contributing to the RHS of Eq. 22 between the two triangle diagrams and the two tree-level diagrams in Fig.12 correspond to the interference terms between the four box diagrams in Fig.2 and the tree-level diagram in Fig.1. The other two interference terms of the fermion loop diagram with the two tree-level graphs in Fig.12 correspond to those of the triangle diagrams in Fig.2 with the tree-level diagrams in Fig.1. The relative minus sign on the RHS of Eq. 22 can be explained as following. We must add a minus sign to the amplitude for Fig.12e due to the closed fermion loop. Such a minus sign is absent in the corresponding amplitude in Fig.2. On the contrary, there is a minus sign in front of the box diagram in Fig.2. No such minus sign is present in Fig.12.c, d. Thus, the CPT relation Eq. 22 manifests itself through the Cutkosky rule in Eq. 15.

## 6 Summary

In this work we considered the CP asymmetries induced by MSSM new phase in the semi-leptonic three body decays of the top quark under such an assumption that the top squark is so heavy that no CP-odd effects are observable in top quark two body decays in one-loop level. In our calculation  $A_{CP}$  can reach up to 0.55% in the most favorable case. Considering the small total branch ratio for  $\sqrt{q^2} > 100GeV$  which is about  $\frac{1}{100}$  for all three body decays it is really hard to detect such small effects experimentally.

However, several constraint in our calculations can be relaxed. For example, the gaugino mass parameters  $m_1$  and  $m_2$  can be complex and give new CP-violating sources if we do not make the universal assumption about the gauginos masses in GUT scale. Another possible CP source is from the Higgs mass parameter  $\mu$ . According to recent studies on the neutron EDM, cancellation among different contributions can take place so that  $\mu$  can have large imaginary part even when super particles are in  $\mathcal{O}(100GeV)$  level[14]. If this is the case, complex  $\mu$  can introduce additional CP asymmetries in top quark decays. And, if we relax the constraint on the  $m_{\tilde{t}_1}$  to be slightly above 100GeV,  $m_{\tilde{t}_1}$  and  $m_{\chi^0}$  cut can also give contribution to  $A_{CP}$  in three body decays. Another improvement may come from branch ratio enhancement. The direct experimental constraint on  $m_{\chi^0} + m_{\chi^+}$  is even below  $m_W$  today [5]. As  $\sqrt{q^2}$  decrease the branch ratio for top quark three body decay increase rapidly (e.g., the branch ratio for all three body decays is about  $\frac{1}{35}$  for  $\sqrt{q^2} > 90GeV$ ). So, if  $m_{\chi^0} + m_{\chi^+}$  is not much heavier than  $m_W$ , the  $A_{CP}$  in the three body decay is hopefully detectable in the LHC which may be able to produce  $10^7 t\bar{t}$  pairs.

On the contrary, if  $m_{\chi^+}$  and  $m_{\tilde{t}}$  are both heavier than, e.g., 140GeV, all the windows for CP asymmetries induced by super particles will be shut up. CP-odd effects in top quark decays induced by MSSM particles can only exist beyond one-loop order. This will be beyond the experiment ability in the near future.

## Appendix A

There are different conventions for super particles mass matrices adopted in literature so that it is very easy to make sign errors. To avoid sign errors we rederived the MSSM Lagrangian. For most part we adopted the same conventions described by J. Rosiek[8]. The original MSSM Lagrangian is given by Eq. 1—Eq. 6 of which all fields are gauge eigenstates. We should point out that the  $\epsilon_{12} = -1$  convention will give an extra minus sign to parameter  $\mu$  compared to those adopted the convention  $\epsilon_{12} = 1$  (if universal relation for gauginos is taken only relative sign between the gauginos and  $\mu$  is significant). To get the physical spectrum of particles one should carry out the standard procedure of gauge symmetry breaking. After SSB super-particles will mix and form different mass eigenstates.

The charged Higgsinos and charged winos mix and give two mass eigenstates named charginos. The mass matrix of charginos is

$$M_\chi = \begin{bmatrix} m_2 & \sqrt{2}M_W \sin \beta \\ \sqrt{2}M_W \cos \beta & \mu \end{bmatrix} . \quad (\text{A.1})$$

The mixing matrices satisfy

$$(Z^-)^T M_\chi Z^+ = \text{diag} (m_{\chi_1}, m_{\chi_2}) , \quad (\text{A.2})$$

and is defined by

$$\begin{pmatrix} -i \lambda^- \\ \psi_{H_1}^2 \end{pmatrix} = Z^- \begin{pmatrix} \varphi_1^- \\ \varphi_2^- \end{pmatrix} , \quad (\text{A.3})$$

$$\begin{pmatrix} -i \lambda^+ \\ \psi_{H_2}^1 \end{pmatrix} = Z^+ \begin{pmatrix} \varphi_1^+ \\ \varphi_2^+ \end{pmatrix} . \quad (\text{A.4})$$

In the above equations  $\lambda^\pm = \frac{1}{\sqrt{2}}(\lambda_W^1 \mp i\lambda_W^2)$  where  $\lambda_W^{1,2}$  are the first and second components of wino as in Eq. 5.  $\psi_{H_1}^2$  is the first (or up) Fermion component of the second Higgs super field doublet. The fields on the left hand side of the above equations are gauge eigenstates and the fields on the right hand side are mass eigenstates. The four-component Dirac spinor charginos are defined by  $\chi_i^+ = \begin{bmatrix} \varphi_i^+ \\ \varphi_i^- \end{bmatrix}$ . The mass term which will appear in the final form of Lagrangian is  $-m_{\chi_i} \bar{\chi}_i \chi_i$ .

The third component of wino, photino and neutral Higgsinos combine to give four Majorana neutralinos. The mass matrix for neutralinos is

$$M_{\chi^0} = \begin{bmatrix} m_1 & 0 & -M_Z \cos \beta \sin \theta_W & M_Z \sin \beta \sin \theta_W \\ 0 & m_2 & M_Z \cos \beta \cos \theta_W & -M_Z \sin \beta \cos \theta_W \\ -M_Z \cos \beta \sin \theta_W & M_Z \cos \beta \cos \theta_W & 0 & -\mu \\ M_Z \sin \beta \sin \theta_W & -M_Z \sin \beta \cos \theta_W & -\mu & 0 \end{bmatrix}, \quad (\text{A.5})$$

which is diagonalized by

$$Z_N^T M_{\chi^0} Z_N = \text{diag} (m_{\chi_1^0}, m_{\chi_2^0}, m_{\chi_3^0}, m_{\chi_4^0}) . \quad (\text{A.6})$$

$Z_N$  is defined by

$$\begin{pmatrix} -i\lambda_B \\ -i\lambda_W^3 \\ \psi_{H_1}^1 \\ \psi_{H_2}^2 \end{pmatrix} = Z_N \begin{pmatrix} \varphi_1^0 \\ \varphi_2^0 \\ \varphi_3^0 \\ \varphi_4^0 \end{pmatrix}, \quad (\text{A.7})$$

where  $\lambda_B$  is photino. All fields on the left hand side of the above equation are gauge eigenstate and those on the right hand side are mass eigenstates. The four-component Dirac spinor form for neutralino is  $\chi_i^0 = \begin{bmatrix} \varphi_i^0 \\ \varphi_i^0 \end{bmatrix}$ . The mass term in the final form of Lagrangian of neutralino is  $-\frac{1}{2}m_{\chi_i^0}\chi_i^0\bar{\chi}_i^0$ .

Ignoring generation mixing, the mass eigenstates of squarks are obtained by mixing the left-handed and right-handed eigenstates of squarks. Its mass matrix is

$$\begin{aligned} M_f^2 &= \begin{bmatrix} L_f & C_f \\ C_f^* & R_f \end{bmatrix} \\ L_f &= m_f^2 + \cos 2\beta(T_{3f} - Q_f \sin^2 \theta_W)M_Z^2 + m_{f_L}^2 \\ R_f &= m_f^2 + \cos 2\beta Q_f \sin^2 \theta_W M_Z^2 + m_{f_R}^2 \\ C_f &= -m_f(r_f \mu + A_f^*) = |C_f|e^{i\phi_f} \end{aligned} \quad (\text{A.8})$$

where  $T_{3f}$  is  $\frac{1}{2}$  for up squark and  $-\frac{1}{2}$  for down squark.  $Q_f$  is the charge of the sparticle and  $r_f$  is  $\cot \beta$  for up squark and  $\tan \beta$  for down squark.  $m_{f_L}^2, m_{f_R}^2, A_f$  are the corresponding diagonal elements of  $m_Q^2, m_U^2(m_D^2)$  and  $A_U(A_D)$  in  $\mathcal{L}_{\text{soft}}$ , respectively. The mixing matrix satisfies

$$Z_f^\dagger M_f^2 Z_f = \text{diag} (m_{f_1}^2, m_{f_2}^2). \quad (\text{A.10})$$

They are defined, e.g., for up squark, by

$$\begin{pmatrix} \tilde{Q}_L^U \\ \tilde{U}_R^* \end{pmatrix} = Z_U \begin{pmatrix} \tilde{U}_1 \\ \tilde{U}_2 \end{pmatrix}, \quad (\text{A.11})$$

where  $\tilde{Q}_L^U$  is the up component of left-handed up squark doublet,  $\tilde{U}_R$  is the right-handed up squark.  $\tilde{U}_{1,2}$  are the two mass eigenstates of up squark. The conjugate of  $\tilde{U}_R$  in Eq. A.11 comes from that we adopt the charge conjugate of left hand Fermion to represent its right hand component in the original MSSM Lagrangian. The final form of squark mass term in Lagrangian is  $-m_{\tilde{U}_i}^2 \tilde{U}_i^* \tilde{U}_i$ . In particular, the mixing matrix for top squark is given by

$$Z_t = \begin{bmatrix} \cos \theta_t e^{i\phi_t/2} & -\sin \theta_t e^{i\phi_t/2} \\ \sin \theta_t e^{-i\phi_t/2} & \cos \theta_t e^{-i\phi_t/2} \end{bmatrix}, \quad (\text{A.12})$$

where  $\phi_t$  is defined in (A.9) and

$$\begin{aligned} \tan \theta_t &= \frac{2|C_t|}{L_t - R_t - \sqrt{\Delta}}, \\ \Delta &= (L_t - R_t)^2 + 4|C_t|^2. \end{aligned} \quad (\text{A.13})$$

The formulae for down squark are similar to up squark. Note the definition of mixing matrix for down squark given by [8] is the complex conjugate of the mixing matrix given here.

## Appendix B

In this appendix we list the relevant pieces of the SUSY Lagrangian in terms of the mass eigenstates[8].

$$\mathcal{L}_{t\tilde{t}\chi^0} = g\tilde{t}_i^* \bar{\chi}_j^0 [A^{ij} P_L + B^{ij} P_R] t + H.C. \quad (\text{B.1})$$

$$\mathcal{L}_{b\tilde{t}\chi} = g\tilde{t}_i \bar{b} [C^{ij} P_L + D^{ij} P_R] V_{tb}^* \chi_j^c + H.C. \quad (\text{B.2})$$

$$\mathcal{L}_{b\tilde{b}\chi^0} = g\tilde{b}_i^* \bar{\chi}_j^0 [E^{ij} P_L + F^{ij} P_R] b + H.C. \quad (\text{B.3})$$

$$\mathcal{L}_{t\tilde{b}\chi} = g\tilde{b}_i \bar{\chi}_j [G^{ij} P_L + H^{ij} P_R] V_{tb}^* t + H.C. \quad (\text{B.4})$$

$$\mathcal{L}_{\tau\tilde{\tau}\chi^0} = g\tilde{\tau}_i^* \bar{\chi}_j^0 [M^{ij} P_L + N^{ij} P_R] \tau + H.C. \quad (\text{B.5})$$

$$\mathcal{L}_{\nu\tilde{\tau}\chi} = gU^{ij} \tilde{\tau}_i^* \bar{\chi}_j P_L \nu_\tau + H.C. \quad (\text{B.6})$$

$$\mathcal{L}_{\tau\tilde{\nu}\chi} = -g\tilde{\nu}_\tau^* \bar{\chi}_i^c [Z_{1i}^+ P_L + l^\tau Z_{2i}^{*-} P_R] + H.C. \quad (\text{B.7})$$

$$\mathcal{L}_{\nu\tilde{\nu}\chi^0} = gW_i \tilde{\nu}_\tau^* \bar{\chi}_i^0 P_L \nu_\tau + H.C. \quad (\text{B.8})$$

$$\mathcal{L}_{\chi\chi^0 W} = g\bar{\chi}_i \nu^\mu [O^{ij} P_L + V^{ij} P_R] \chi^0 W_\mu^+ + H.C. \quad (\text{B.9})$$

where

$$\begin{cases}
A^{ij} = \frac{-1}{\sqrt{2}\cos\theta} Z_t^{1i*} (\frac{1}{3} Z_N^{1j} \sin\theta + Z_N^{2j} \cos\theta) - u^t Z_t^{2i*} Z_N^{4j} \\
B^{ij} = \frac{2\sqrt{2}\sin\theta}{3\cos\theta} Z_t^{2i*} Z_N^{1j*} - u^t Z_t^{1i*} Z_N^{4j*} \\
C^{ij} = -d^b Z_t^{1i} Z_{2j}^- \\
D^{ij} = -Z_t^{1i} Z_{1j}^{+*} + u^t Z_t^{2i} Z_{2j}^{+*} \\
E^{ij} = \frac{-g}{\sqrt{2}\cos\theta} Z_b^{1i} (\frac{1}{3} Z_N^{1j} \sin\theta - Z_N^{2j} \cos\theta) + d^b Z_b^{2i} Z_N^{3j} \\
F^{ij} = \frac{-\sqrt{2}\sin\theta}{3\cos\theta} Z_b^{2i} Z_N^{1j*} + d^b Z_b^{1i} Z_N^{3j*} \\
G^{ij} = -Z_b^{1i} Z_{1j}^- - d^b Z_b^{2i} Z_{2j}^- \\
H^{ij} = u^t Z_b^{1i} Z_{2j}^{+*} \\
M^{ij} = \frac{1}{\sqrt{2}\cos\theta} Z_\tau^{1i} (Z_N^{1j} \sin\theta + Z_N^{2j} \cos\theta) + l^\tau Z_\tau^{1i} Z_N^{3j} \\
N^{ij} = \frac{-\sqrt{2}\sin\theta}{\cos\theta} Z_\tau^{2i} Z_N^{1j*} + l^\tau Z_\tau^{1i} Z_N^{3j*} \\
U^{ij} = -(Z_\tau^{1i} Z_{1j}^- + l^\tau Z_\tau^{2i} Z_{2j}^-) \\
W_i = \frac{1}{\sqrt{2}\cos\theta} (Z_N^{1i} \sin\theta - Z_N^{2i} \cos\theta) \\
\begin{cases}
O^{ij} = Z_N^{2i} Z_{1j}^{+*} - \frac{1}{\sqrt{2}} Z_N^{4j} Z_{2j}^{+*} \\
V^{ij} = Z_N^{2i*} Z_{1j}^- + \frac{1}{\sqrt{2}} Z_N^{3i*} Z_{2j}^-
\end{cases}
\end{cases} \tag{B.10}$$

$u^t$ ,  $d^b$  and  $l^\tau$  are the Yukawa coupling parameters for top, bottom and  $\tau$  respectively. They are given by

$$\begin{aligned}
u^t &= \frac{m_t}{\sqrt{2}m_W \sin\beta} \ , \\
d^b &= \frac{-m_b}{\sqrt{2}m_W \cos\beta} \ , \\
l^\tau &= \frac{-m_\tau}{\sqrt{2}m_W \cos\beta} \ .
\end{aligned} \tag{B.11}$$

The vertex in Eq. B.9 can be expressed as

$$\mathcal{L}_{\chi\chi^0 W} = -g\chi_j^c \nu^\mu [O^{ij*} P_R + V^{ij*} P_L] \chi_i^0 W_\mu^- + H.C. \tag{B.12}$$

which can be used to read off the Feynman rule directly for the Fig.2e.

## Appendix C

In this section we give the formulae for the quantity  $\frac{1}{2}\sum\Delta|M|^2$  in Eq. 17 for Fig. 2c and 2e in detail. In the following formulae the  $\mathcal{X}^i$ s are not separated out explicitly as in Eq. 17 for convenience. All the formulae and variables are given in the  $\vec{q} = 0$  system. The imaginary part of the amplitude for Fig2.c is

$$ImA(c) = \frac{g^4}{2(2\pi)^2} \int \frac{d^3k}{2E} \delta((q-k)^2 - m_\chi^2) \ .$$

$$\frac{\bar{u}(p_\nu)\Gamma_{\bar{\nu}\nu\chi^0}(\not{k} + m_{\chi^0})\Gamma_{\bar{t}t\chi^0}u(p_t)\bar{u}(p_b)\Gamma_{\bar{b}b\chi}(\not{q} - \not{k} - m_\chi)\Gamma_{\bar{\nu}\tau\chi}v(p_\tau)}{[(p_t - k)^2 - m_t^2] [(p_\nu - k)^2 - m_\nu^2]} \quad (\text{C.1})$$

where  $k = (E, \vec{k})$  is the four-momenta of  $\chi^0$  and the  $\Gamma$ 's are interaction vertex factors. The quantity  $\frac{1}{2} \sum_{spin} \Delta|M|^2$  for Fig.2c is

$$\begin{aligned} \frac{1}{2} \sum \Delta|M|^2(c) = & \frac{g^6}{q^2 - m_W^2} \frac{|\vec{k}|}{4\pi\sqrt{q^2}} \left\{ \frac{1}{A'a} (2T + LE'_{\nu_\tau} |\vec{k}| \cos \alpha) + \frac{2\rho b \cos \alpha}{A'B'a} \right. \\ & - \frac{a(S + LB'/4) + T + \frac{1}{2}LE'_{\nu_\tau} |\vec{k}| \cos \alpha}{A'a^2} \log \frac{1+a}{1-a} \\ & + \frac{1}{A'B'ab} (-\Omega + \rho(\frac{1}{a} + \frac{1}{b} \cos \alpha)) \log \frac{1-b}{1+b} \\ & \left. + \frac{1}{A'B'} (\Sigma - \frac{\Omega}{a} + \frac{\rho}{a^2}) \frac{1}{\sqrt{K}} \log \frac{1-ab \cos \alpha + \sqrt{K}}{1-ab \cos \alpha - \sqrt{K}} \right\} \quad (\text{C.2}) \end{aligned}$$

where

$$\begin{aligned} \rho &= -2\mathcal{X}_a^2 p_\nu \cdot p_\tau |\vec{k}|^2 |\vec{p}_t|^2 \\ \Omega &= (\mathcal{X}_a^1 m_{\chi^0} m_t - 2\mathcal{X}_a^2 (p_b \cdot p_\nu + k \cdot q)) p_\nu \cdot p_\tau |\vec{k}| |\vec{p}_t| \\ &\quad + 4\mathcal{X}_a^2 p_\nu \cdot p_\tau E E_t |\vec{k}| |\vec{p}_t| - 2T' E'_{\nu_\tau} E - B'T \\ \Sigma &= 2\mathcal{X}_a^1 m_{\chi^0} m_t p_b \cdot p_\nu p_\nu \cdot p_\tau + (2\mathcal{X}_a^2 (p_b \cdot p_\nu + k \cdot q) - \mathcal{X}_a^1 m_{\chi^0} m_t) p_\nu \cdot p_\tau E E_t \\ &\quad + \mathcal{X}_a^1 m_{\chi^0} m_t p_\nu \cdot p_\tau k \cdot q - 2\mathcal{X}_a^2 p_\nu \cdot p_\tau (E E_t)^2 \\ &\quad + 2S' E'_{\nu_\tau} E - L E'_{\nu_\tau} E^2 + B'S + LB'/4 \\ &\quad - \mathcal{X}_a^2 (p_b \cdot p_\nu p_t \cdot p_\tau - p_b \cdot p_t p_\nu \cdot p_\tau + p_t \cdot p_\nu p_b \cdot p_\tau) \\ K &= a^2 + b^2 - a^2 b^2 \sin^2 \alpha - 2ab \cos \alpha \quad (\text{C.3}) \end{aligned}$$

In above formulae,  $E'_{\nu_\tau}$  is the energy of  $p_\nu$  in the  $\vec{q} = 0$  system.  $\alpha$  is the angle between the three-momenta of top quark and  $\nu_\tau$  in the  $\vec{q} = 0$  system.  $q^2$  is the invariant mass square of the final state lepton pair. Other quantities are defined as:

$$\begin{aligned} A &= m_t^2 + m_{\chi^0}^2 - m_t^2, \\ B &= m_{\chi^0}^2 - m_\nu^2, \\ A' &= A - 2E E_t, \\ B' &= B - 2E E'_{\nu_\tau}, \\ a &= \frac{2|\vec{k}| |\vec{p}_t|}{A}, \\ b &= \frac{2E'_{\nu_\tau} |\vec{k}|}{B}, \end{aligned}$$

$$\begin{aligned}
L &= \mathcal{X}_a^2 p_t \cdot p_b, \\
S &= \frac{1}{2} \mathcal{X}_a^1 m_{\chi^0} m_t p_b \cdot q + \mathcal{X}_a^2 p_b \cdot p_\nu p_t \cdot q + \\
&\quad \mathcal{X}_a^2 (p_b \cdot p_\tau - p_t \cdot p_\nu) E E_t + \mathcal{X}_a^2 p_t \cdot p_\nu k \cdot q, \\
T &= \mathcal{X}_a^2 (p_b \cdot p_\tau - p_t \cdot p_\nu) |\vec{k}| |\vec{p}_t|, \\
S' &= \frac{1}{2} \mathcal{X}_a^1 m_{\chi^0} m_t (p_b \cdot p_\tau - p_b \cdot p_\nu) + \mathcal{X}_a^2 p_b \cdot p_\nu p_t \cdot q + \\
&\quad \mathcal{X}_a^2 (p_b \cdot p_\tau + p_t \cdot p_\nu) E E_t - \mathcal{X}_a^2 p_t \cdot p_\nu k \cdot q, \\
T' &= \mathcal{X}_a^2 (p_b \cdot p_\tau + p_t \cdot p_\nu) |\vec{k}| |\vec{p}_t|
\end{aligned} \tag{C.4}$$

The non-Lorentz invariant four-vector component are expressed as

$$\begin{aligned}
E_{\nu_\tau}' &= \frac{\sqrt{q^2}}{2}, \\
E_t &= \frac{m_t^2 + q^2}{2\sqrt{q^2}}, \\
|\vec{p}_t| &= \frac{m_t^2 - q^2}{2\sqrt{q^2}}, \\
E &= \frac{m_t^2 + q^2}{2m_t}, \\
|\vec{k}| &= \sqrt{E^2 - m_{\chi^0}^2}, \\
\cos \alpha &= \frac{m_t^2 + q^2 - 4p_t \cdot p_\nu}{m_t^2 - q^2}
\end{aligned} \tag{C.5}$$

$\mathcal{X}_a^{1,2}$  are given by

$$\mathcal{X}_a^1 = -Im B^{i1} D^{i1} Z_{11}^+ W^{1*}, \quad \mathcal{X}_a^2 = -Im A^{i1} D^{i1} Z_{11}^+ W^{1*} \tag{C.6}$$

The elements of the mixing matrices in the above equation are taken according to that only  $m_{\chi_1^0}$  and  $m_{\chi_1^+}$  are considered in our calculations.

The corresponding formulae for Fig2.e are

$$\begin{aligned}
Im A(e) &= \frac{g^4}{2\sqrt{2}(2\pi)^2} \int \frac{d^3k}{2E} \delta((q-k)^2 - m_\chi^2) \\
&\quad \frac{\bar{u}(p_b) \Gamma_{\bar{\tau} b \chi} (\not{k} - \not{q} + m_\chi) \gamma^\mu \Gamma_{\chi \chi^0 W} \Gamma_{\bar{t} t \chi^0} u(p_t) \bar{u}(p_\nu) \gamma_\mu P_L v(p_\tau)}{(q^2 - m_W^2) [(p_t - k)^2 - m_{\tilde{t}}^2]}
\end{aligned} \tag{C.7}$$

The quantity  $\frac{1}{2} \sum_{spin} \Delta |M|^2$  for fig.2e is

$$\begin{aligned}
\frac{1}{2} \sum \Delta |M|^2 &= \frac{-g^6}{(q^2 - m_W^2)^2} \frac{1}{2\sqrt{2}\pi} \frac{|\vec{k}|}{\sqrt{q^2}} \cdot \\
&\quad \frac{1}{A'a} \left\{ 2\left(Y - \frac{X}{a}\right) + \left(Z - \frac{Y}{a} + \frac{X}{a^2}\right) \log \frac{1+a}{1-a} \right\}
\end{aligned} \tag{C.8}$$

where

$$\begin{aligned}
X &= 2\mathcal{X}_e^3[E'_{\nu_\tau}|\vec{P}_t| \cos \alpha(p_b \cdot p_\tau - p_t \cdot p_\nu) - |\vec{P}_t|^2 p_\nu \cdot p_\tau + \\
&\quad \frac{1}{2}E'_{\nu_\tau}{}^2 \cos^2 \alpha p_t \cdot p_b]|\vec{k}|^2 \\
Y &= \Omega - S|\vec{P}_t||\vec{k}| + TE'_{\nu_\tau} \cos \alpha \\
Z &= \Sigma + SEE_t + T'EE'_{\nu_\tau} + H \\
S &= (2\mathcal{X}_e^3 p_b \cdot p_\nu - \mathcal{X}_e^4 m_{\chi^0} m_t) p_\nu \cdot p_\tau \\
T &= 2\mathcal{X}_e^2 m_\chi m_t p_b \cdot p_\nu - \mathcal{X}_e^4 m_{\chi^0} m_t p_b \cdot p_t - 2\mathcal{X}_e^3 q \cdot p_t p_b \cdot p_\nu \\
T' &= 2\mathcal{X}_e^2 m_\chi m_t p_b \cdot p_\nu - \mathcal{X}_e^4 m_{\chi^0} m_t (p_b \cdot p_\nu - p_b \cdot p_\tau) - \\
&\quad 2\mathcal{X}_e^3 p_b \cdot p_\nu (p_t \cdot p_\nu - p_t \cdot p_\tau) \\
\Omega &= 2\mathcal{X}_e^3 \{-p_b \cdot p_\tau EE'_{\nu_\tau} |\vec{k}| (|\vec{P}_t| + E_t \cos \alpha) + p_t \cdot p_\nu EE'_\tau |\vec{k}| (E_t \cos \alpha - |\vec{P}_t|) \\
&\quad + (2EE_t - k \cdot q) |\vec{P}_t| |\vec{k}| p_\nu \cdot p_\tau - k \cdot q E'_{\nu_\tau} |\vec{k}| \cos \alpha_0 \cdot p_\nu \} \\
\Sigma &= 2\mathcal{X}_e^3 \{E^2 E_t E'_{\nu_\tau} (p_b \cdot p_\tau + p_t \cdot p_\nu) - EE'_\tau k \cdot q p_t \cdot p_\nu - \\
&\quad (EE_t - k \cdot q) EE_t p_\nu \cdot p_\tau - E'_{\nu_\tau} (E^2 - \frac{1}{2}|\vec{k}|^2) p_t \cdot p_b \} \\
H &= \mathcal{X}_e^4 m_{\chi^0} m_t p_\nu \cdot p_\tau k \cdot q + 2(\mathcal{X}_e^1 m_{\chi^0} m_\chi p_t \cdot p_\tau + \mathcal{X}_e^4 m_{\chi^0} m_t p_\nu \cdot p_\tau) p_b \cdot p_\nu \\
&\quad - \mathcal{X}_e^3 m_{\chi^0}^2 (p_b \cdot p_\nu p_t \cdot p_\tau - p_b \cdot p_t p_\nu \cdot p_\tau + p_t \cdot p_\nu p_b \cdot p_\tau)
\end{aligned} \tag{C.9}$$

The parameters  $\mathcal{X}_e^i$ s are given by

$$\begin{aligned}
\mathcal{X}_e^1 &= Im A^{i1} D^{i1} (-V^{11*}), & \mathcal{X}_e^2 &= Im B^{i1} D^{i1} (-V^{11*}), \\
\mathcal{X}_e^3 &= Im A^{i1} D^{i1} (-O^{11*}), & \mathcal{X}_e^4 &= Im B^{i1} D^{i1} (-O^{11*}).
\end{aligned} \tag{C.10}$$

From the above expressions and the expressions for A, D in Eq. B.10 we can see that the  $\mathcal{X}$ s are proportional to  $\xi_t^i = Im(Z_t^{1i*} Z_t^{2i})$  as pointed out in section 3.



## References

- [1] S. Bar-Shalom and G. Eilam, hep-ph/9810234 and references therein.
- [2] B. Grzadkowski and W. Y. Keung, Phys. Lett. B **319**, 526 (1993).
- [3] E. Christova and M. Fabbrichesi, Phys. Lett. B **320**, 299 (1994).
- [4] S. Bar-Shalom, D. Atwood and A. Soni, Phys. Rev. D **57**, 1495 (1998).
- [5] Particle Data Group, Eur. Phys. J. **C3**, 1 (1998).
- [6] W. Fischler, S. Paban and S. Thomas, Phys. Lett **B289**, 373(1992);  
S. M. Barr, Int. J. Mod. Phys. **A8**, 209, (1993);  
T. Farlk, Nucl. Phys. Proc. Suppl. **52**, 78 (1997).
- [7] H. E. Haber and G. L. Kane, Phys. Rep. **117**, 75 (1985);  
H. P. Nilles, Phys. Rep. **110**, 1 (1984).
- [8] J. Rosiek, Phys. Rev. D **41**, 3464 (1990).
- [9] S. Dimoulouos and S. Thomas, Nucl. Phys. B **465**, 23 (1996)
- [10] Y. Nir and N. Seiberg, Phys. Lett. **B309**, 337 (1993).
- [11] J. D. Bjorken and S. D. Drell, *Relativistic Quantum Mechanics*,  
chapter 8, McGraw-Hill, New York, 1964.
- [12] H. Simma, G. Eilam and D. Wyler, Nucl. Phys. B **352**, 367 (1991)
- [13] V. Berger and P. Ohmann, Phys. Rev. D **49**, 4908 (1994).
- [14] Michal Brhlik, Gerald J. Good and G. L. Kane, hep-ph/9810457

## Figure Captions

**FIG. 1** The tree-level Feynman diagram for the process  $t \rightarrow b\nu_\tau\bar{\tau}$ .

**FIG. 2** The SUSY induced CP-violating one-loop diagrams for the process  $t \rightarrow b\nu_\tau\bar{\tau}$ .

**FIG. 3** The CP asymmetry  $A_{CP}$  is plotted as a function of  $\arg(A_t)$  for  $\tan\beta = 1.2$ ,  $m_2 = 150\text{GeV}$ ,  $\mu = -40\text{GeV}$ ,  $M = 200\text{GeV}$ ,  $c=0.2$ . When  $m_{\tilde{t}_1} = 150\text{GeV}$ ,  $A_{CP}$  reaches its maximum.

**FIG. 4** The quantity  $f_{CP}$  defined in Eq. 18 is plotted as function of  $\arg(A_t)$ . All the parameters are the same as that of Fig.3.

**FIG. 5** The CP asymmetry  $A_{CP}$  is plotted as a function of SUSY parameter  $\mu$ , for several values of  $m_2$ , for  $\tan\beta = 1.2$ ,  $M = 160\text{GeV}$ ,  $c=0.15$ ,  $\arg(A_t) = 0.5\pi$ .

**FIG. 6** The CP asymmetry  $A_{CP}$  is plotted as a function of SUSY parameter  $\mu$ , for several values of  $m_2$ ,  $\tan\beta = 5$ . All the other parameters are the same as that of Fig.3.

**FIG. 7** The CP asymmetry  $A_{CP}$  is plotted as a function of SUSY parameter  $\mu$ , for several values of  $m_2$ ,  $\tan\beta = 15$ . All the other parameters are the same as that of Fig.3.

**FIG. 8** The CP asymmetry  $A_{CP}$  is plotted as a function of  $\tan\beta$ , for several values of  $m_2$ ,  $\mu = -70\text{GeV}$ ,  $M = 160\text{GeV}$ ,  $c=0.15$ ,  $\arg(A_t) = 0.5\pi$ .

**FIG. 9** The CP asymmetry  $A_{CP}$  is plotted as a function of  $\tan\beta$ , for several values of  $m_2$ ,  $\mu = -50\text{GeV}$ ,  $M = 160\text{GeV}$ ,  $c=0.15$ ,  $\arg(A_t) = 0.5\pi$ .

**FIG. 10** The CP asymmetry  $A_{CP}$  is plotted as a function of  $m_2$  for  $M = 160\text{GeV}$ ,  $c=0.15$ ,  $\arg(A_t) = 0.5\pi$ ,  $\mu = -50\text{GeV}$  for  $\tan\beta = 2$  and  $\mu = -60\text{GeV}$  for  $\tan\beta = 5, 10$ .

**FIG. 11** The CP asymmetry  $A_{CP}$  is plotted as a function of the mass of the light top squark, for different values of  $m_2$ ,  $\tan\beta = 2.5$ ,  $\mu = -50\text{GeV}$ ,  $\arg(A_t) = 0.5\pi$ .

**FIG. 12** The tree-level and one-loop Feynman diagrams for the process  $t \rightarrow b\chi^0\chi^+$ .

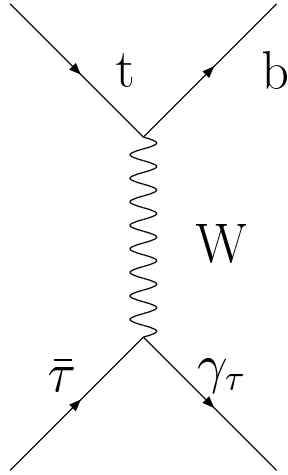


Fig.1

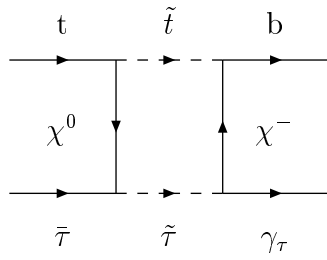


Fig.2a

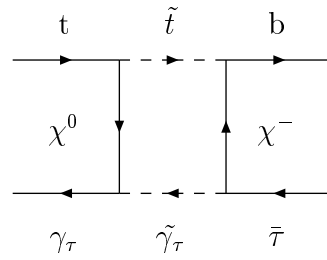


Fig.2b

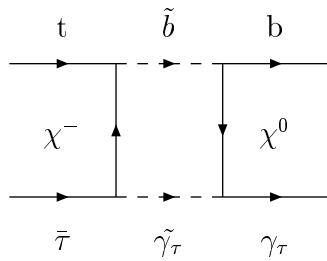


Fig.2c

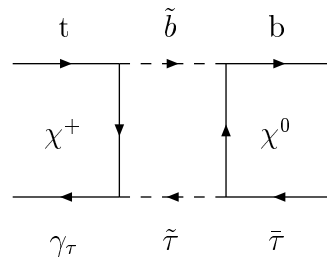


Fig.2d

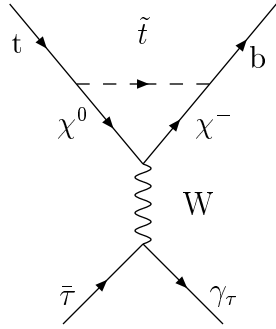


Fig.2e

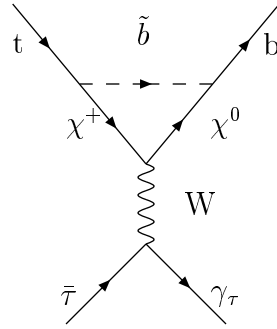


Fig.2f

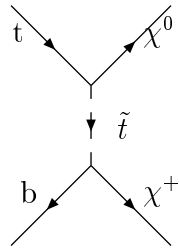


Fig. 12a

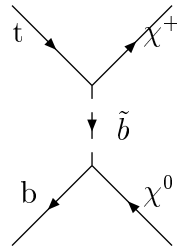


Fig. 12b

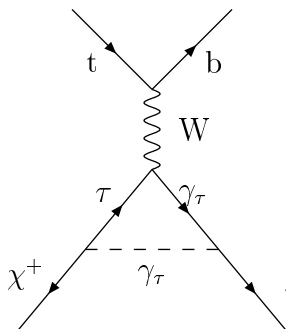


Fig. 12c

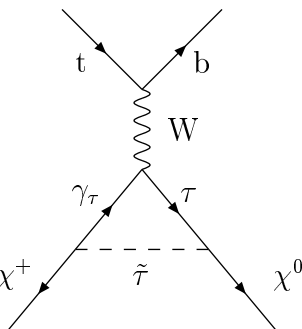


Fig. 12d

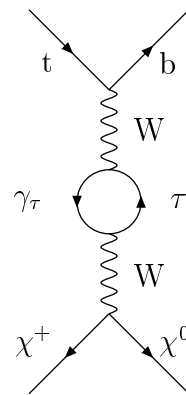


Fig. 12e

Fig. 3

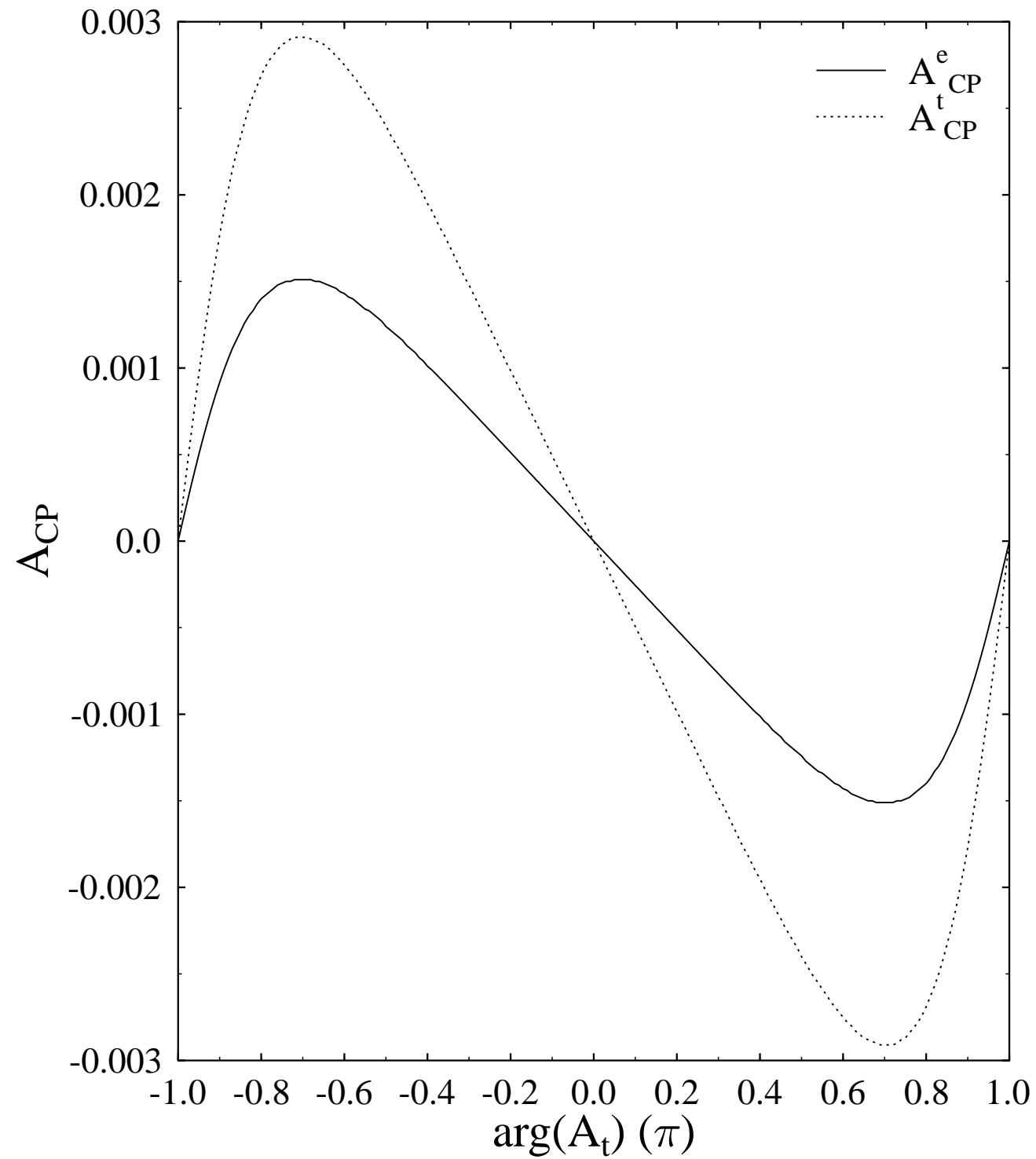


Fig. 4

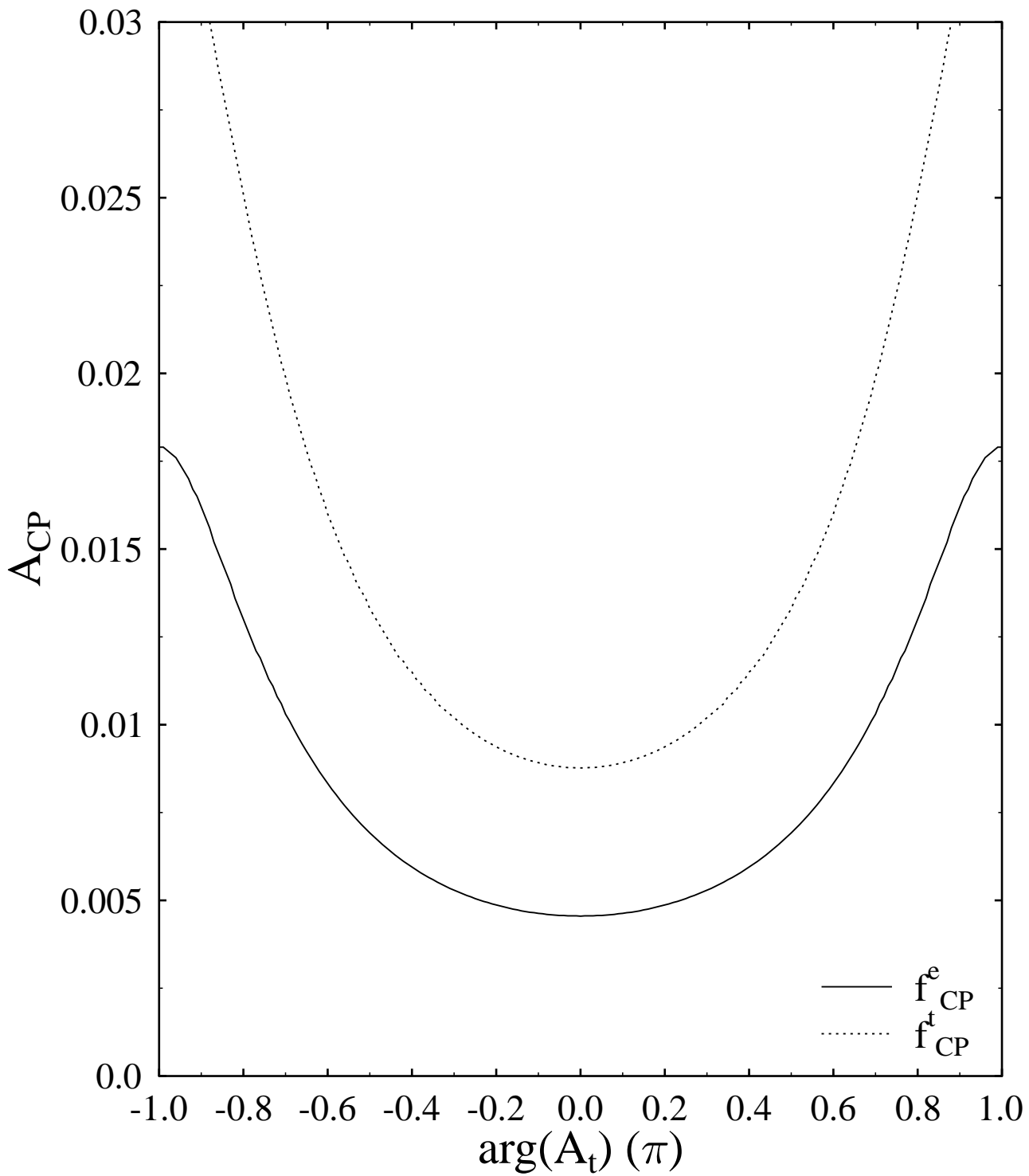


Fig. 5

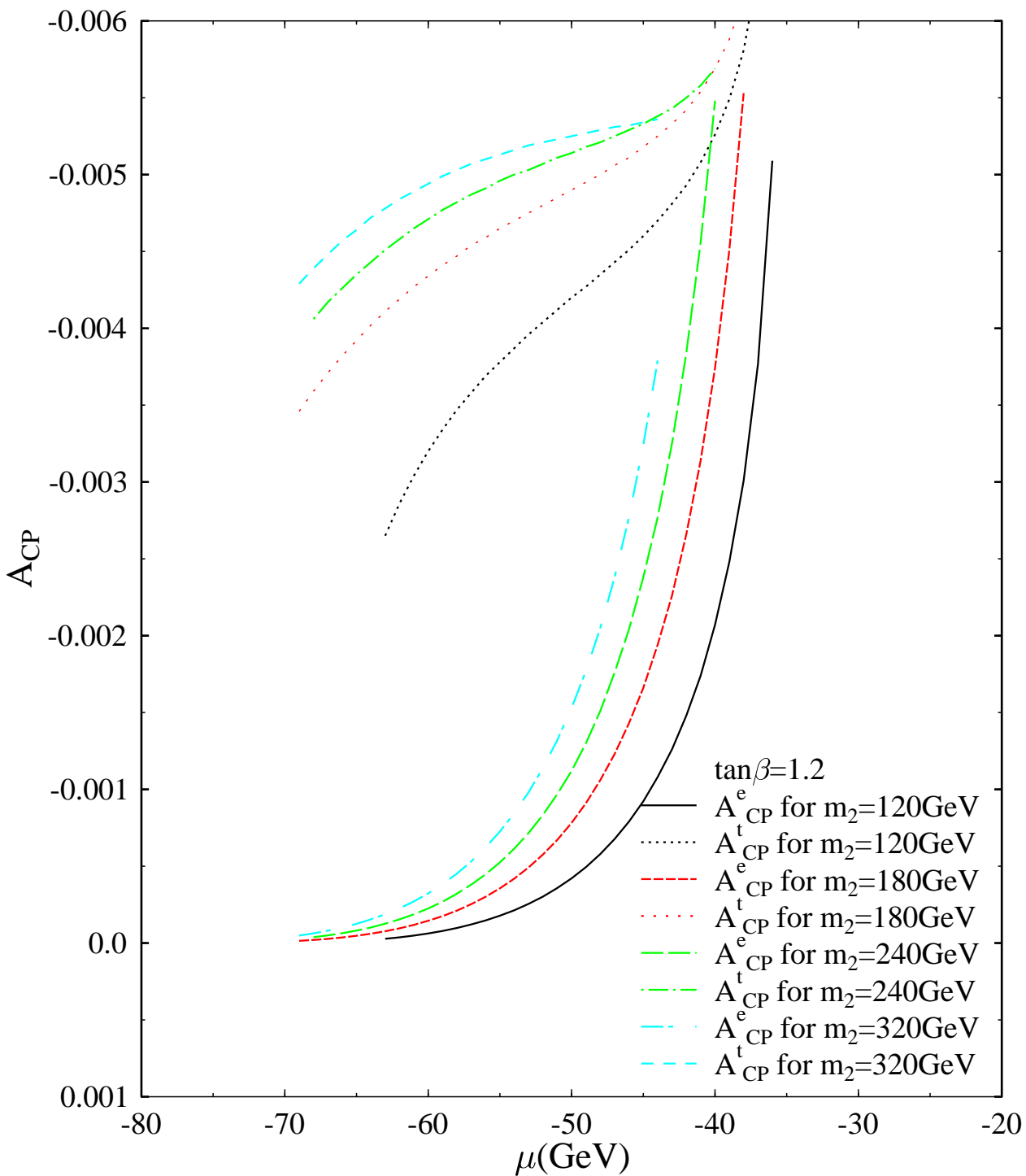


Fig. 6

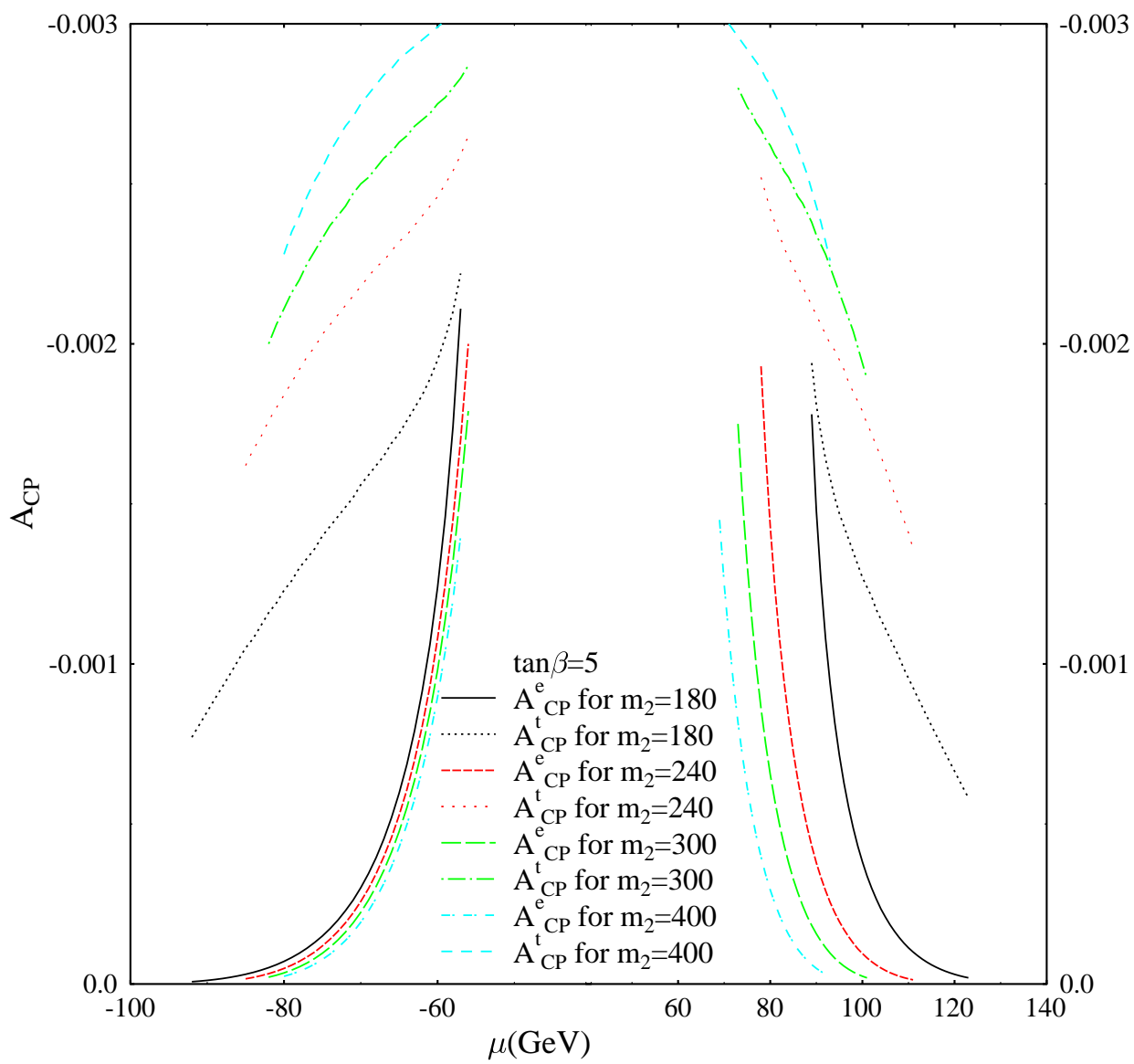




Fig. 7

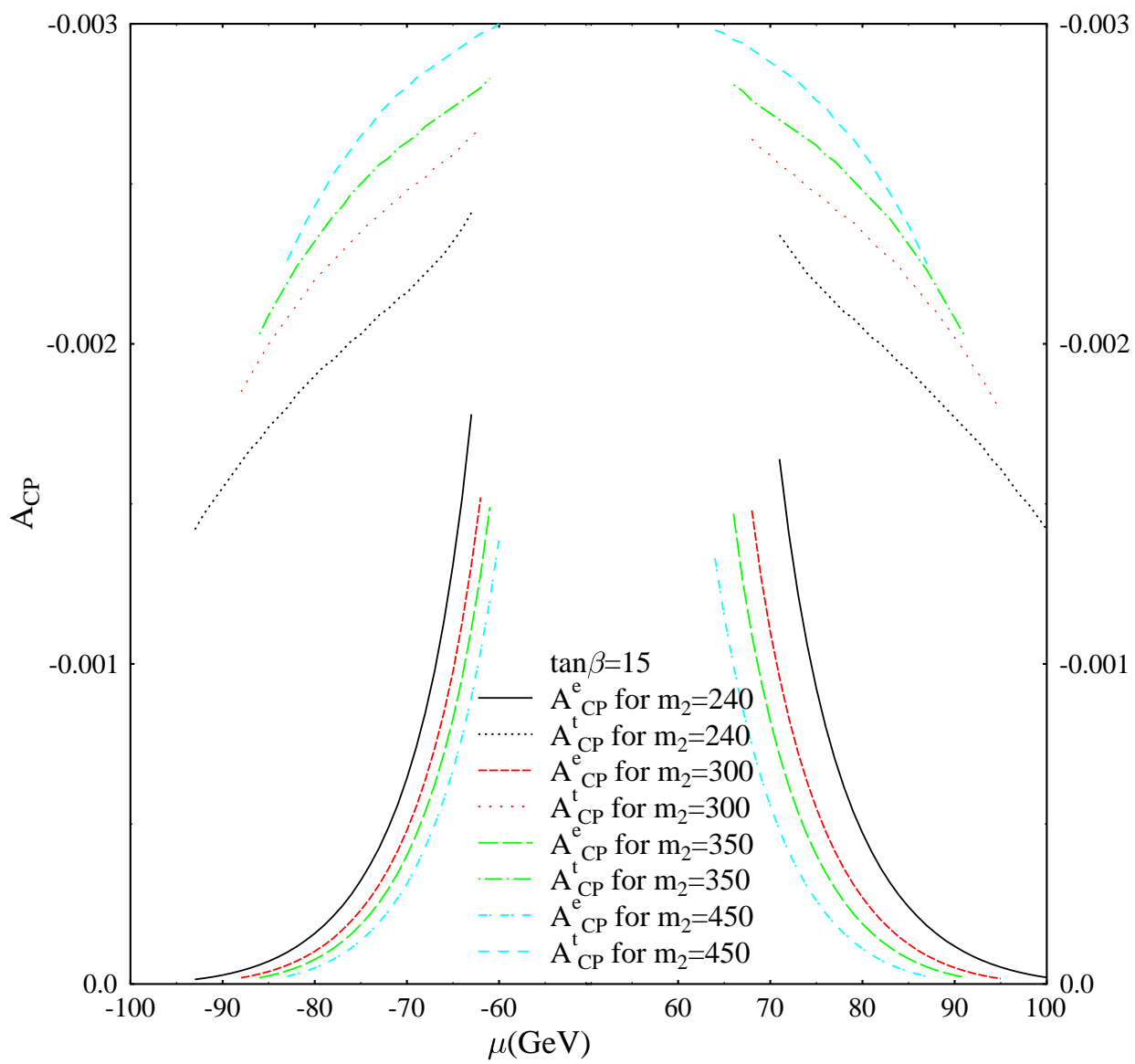


Fig. 8

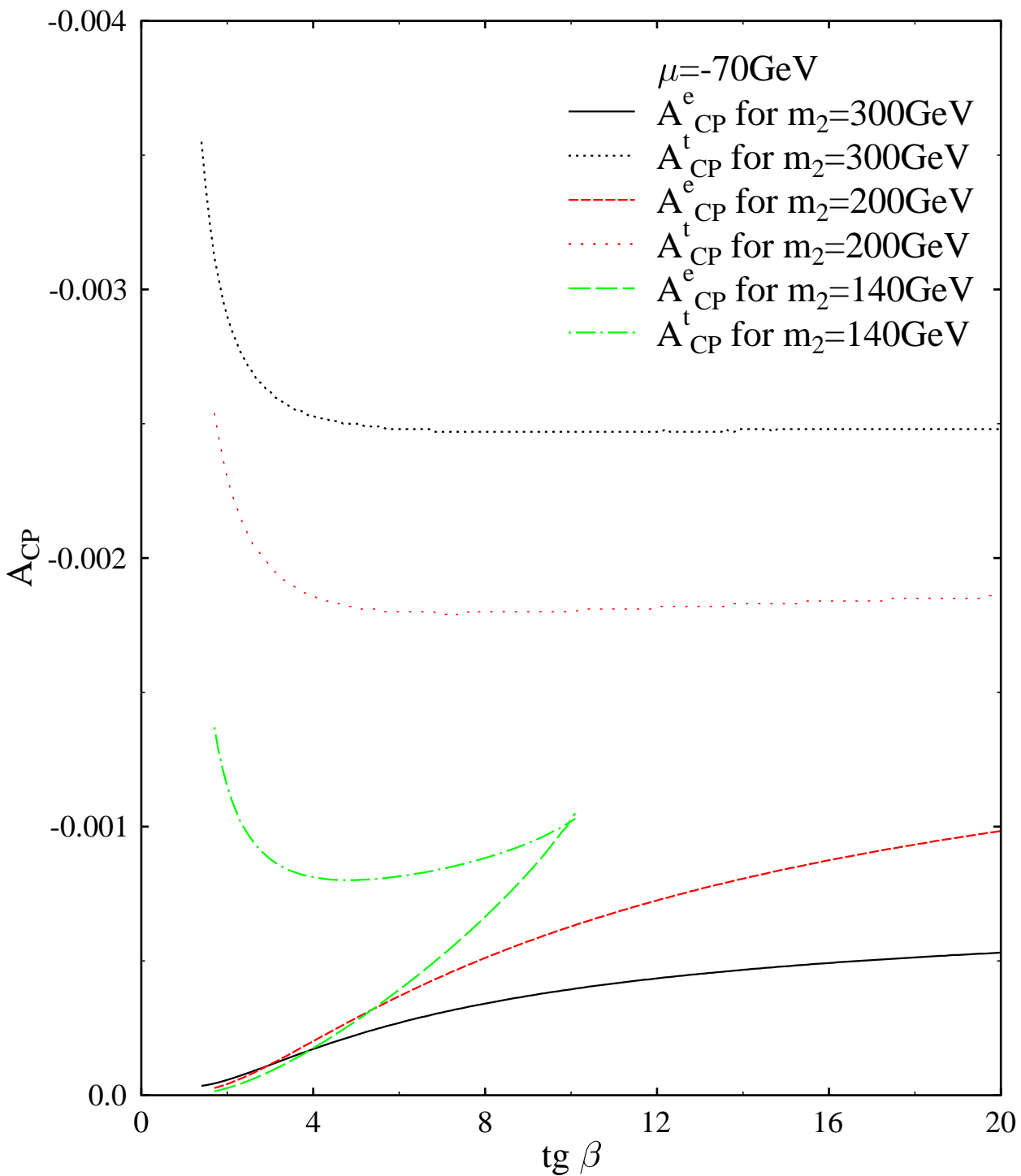


Fig. 9

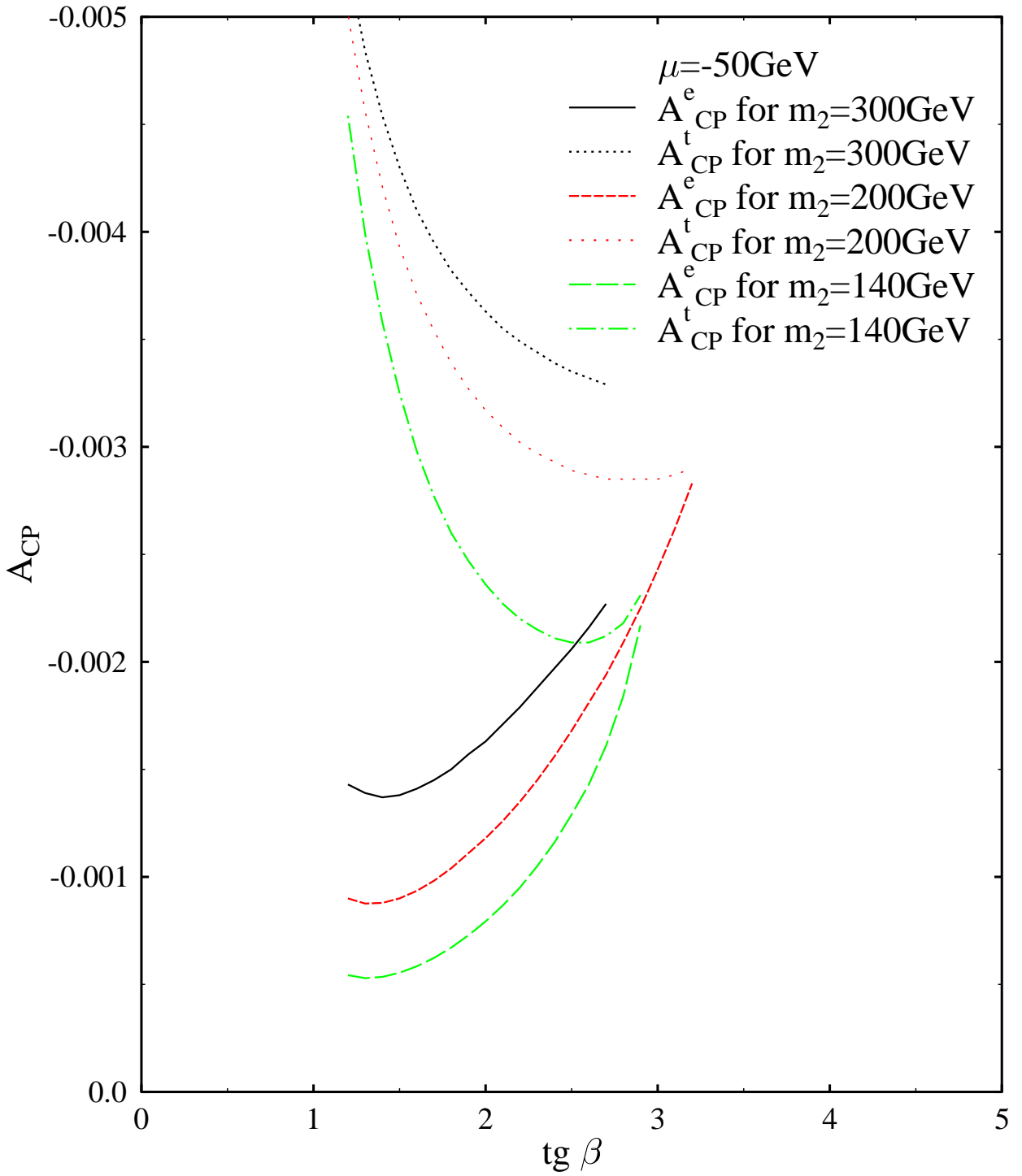


Fig. 10

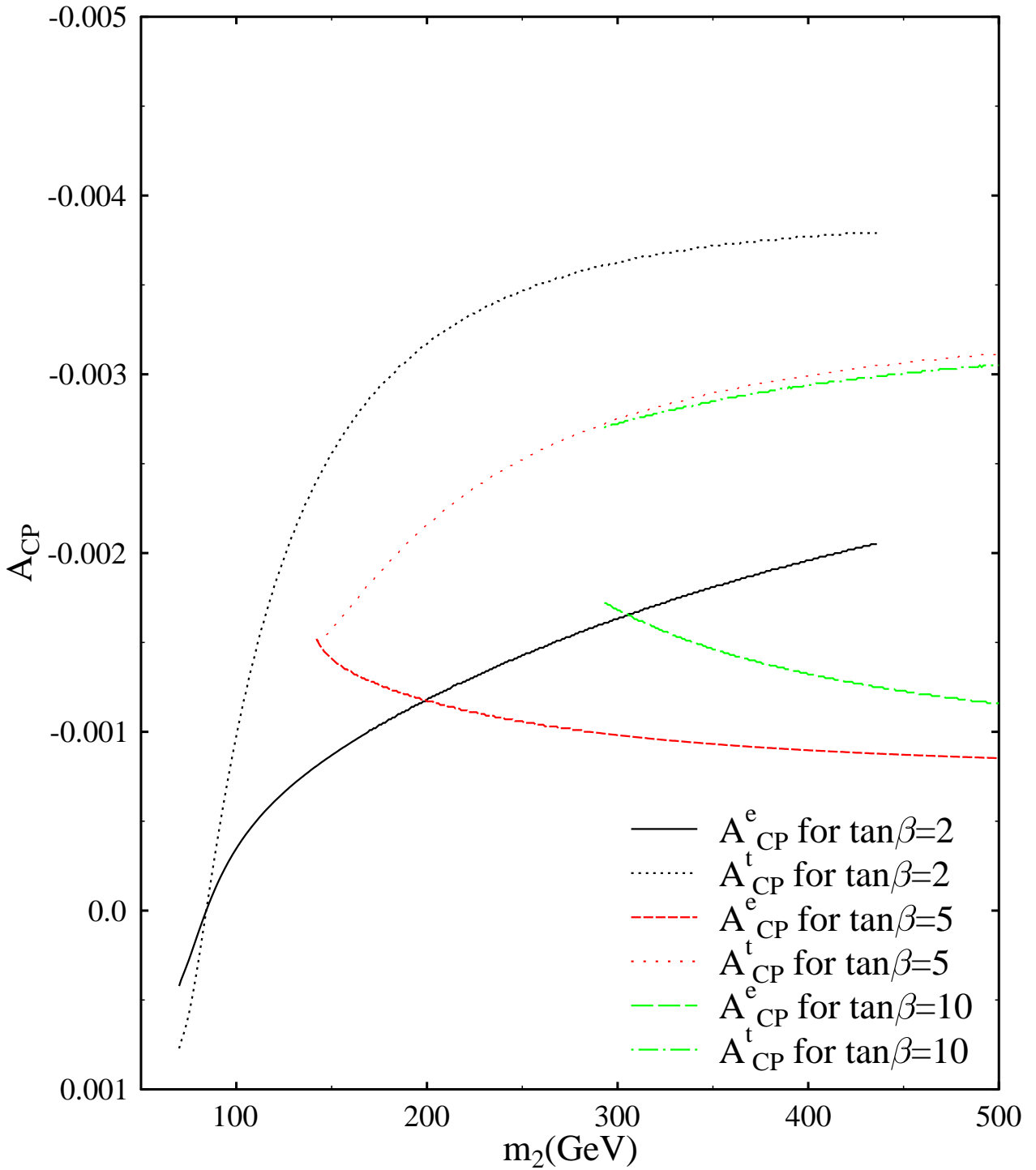


Fig. 11

